Joint 3D inversion of muon tomography and gravity data

Kristofer Davis[1], *Douglas W. Oldenburg*[1], *Vlad Kaminski*[1], *Mark Pilkington*[2], *Douglas Bryman*[3,4], *James Bueno*[4], *and Zhiyi Liu*[4]

[1] *UBC-Geophysical Inversion Facility, Department of Earth and Ocean Sciences, University of British Columbia*

[2] *Geological Survey of Canada*

[3] *Department of Physics and Astronomy, University of British Columbia*

[4] *Advanced Applied Physics Solutions, Inc.*

SUMMARY

Cosmic rays of muons are a natural, abundant, highly-penetrating particle flux that continuously shower the earth's surface and penetrate hundreds of meters underground. Muons are attenuated as they pass through matter so that flux below ground is dependent on the total integrated mass traversed by the particles. Recently, sensors have been placed in existing tunnels to observe the muon flux for brown-field mining applications. We have developed an algorithm to invert muon tomography data, along with gravity data, to recover a 3D distribution of density contrast. The difference in physics between muon ray-paths and gravity data provides a unique insight into the subsurface.

INTRODUCTION

Cosmic rays penetrate the upper atmosphere and create pions, which then decay to muons. The muons travel in approximately straight ray paths and decay in proportion to the amount of matter they pass through. Sensors have been developed to measure the angular distribution of muon flux underground and the flux information provides a link to mass distribution above the detector.

An early application of muon radiography involved searching for hidden chambers in pyramids on the Giza Plateau outside of Cairo, Egypt (Alvarez et al., 1970). Recent application has focussed on the detection of high-density fissile material in containers (e.g. Priedhorsky et al. (2003); Schultz et al. (2004); Wang et al. (2009)) and measurements on the magma chambers of volcanoes (e.g.Tanaka et al. (2010)). The motivation of this paper stems from the current collection of muon data in geophysical applications. Sensors have been deployed for the re-evaluation of models associated with established deposits (i.e. brown-field scenarios). Detectors are placed at depths below and near the deposit (see Figure 1(a) for illustration) in existing tunnels. The key advantage of muon data is that they are directly related to the density along a straight ray from the surface to the detector. Muon data therefore have more localized information about the density than do usual gravity data but an inversion is still required.

In this paper we outline the basics of the muon density survey and develop an inversion algorithm. As with any geophysical technique, additional information can greatly reduce inherent non-uniqueness and we illustrate this by jointly inverting the muon data with conventional gravity data. Muons and gravity data are both linear functionals of density but the associated sensitivity functions are substantially different. The two data sets provide complementary information. A synthetic example illustrates the different types of data and the recovered model of density. Data from a field example are inverted and we also discuss practicalities of the field survey.

MUON TOMOGRAPHY

Sensors observe muon flux as a function of angle over a period of time. The length of time needed for measurements increases with sensor depth because the muon flux is attenuated exponentially with depth. The data are then processed to an integrated path length as a function of a ray-path vector. Angles are binned approximately every 5° within two principal angles: the dip and azimuth (θ and φ, respectively) as shown in Figure 1(b). The geometric length is the distance from the surface to the detector at these two angles in space. These processed data are directly related to the amount of mass along the ray path. The i^{th} datum, d_i, is then a function of the i^{th} ray's true geometric length, P_l^i, from the surface and the density, ρ, throughout that path such that

$$d_i = \int_{P_l^i} \rho(l) dl. \tag{1}$$

In our mathematical representation the earth volume has an upper surface that is determined by the topography and extends deep and wide enough to encompass all ray paths. This volume is discretized into m prismatic cells with constant density. The density becomes a function of three-dimensional space via a vector $\boldsymbol{\rho} = (\rho_1 \dots \rho_m)^T$. Equation 1 is discretized as

$$d_i = \sum_{j=1}^{m} \mathbf{G}_{ij} \rho_j, \tag{2}$$

where $\mathbf{G}_{ij}$ is the geometric length of the i^{th} ray path through the j^{th} volume with the density ρ_j and the data have units of m·g/cm^3. The coefficient matrix $\mathbf{G}$ is often referred to the sensitivity matrix. Equation 2 is expressed in vector notation as

$$\mathbf{d} = \mathbf{G}\boldsymbol{\rho}. \tag{3}$$

These equations can be worked with directly, or they can be reduced to anomalous data by introducing a background density

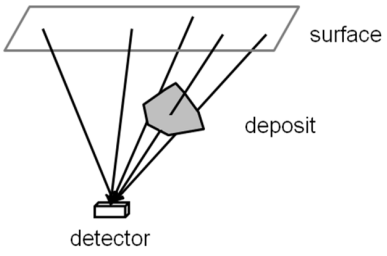

(a)

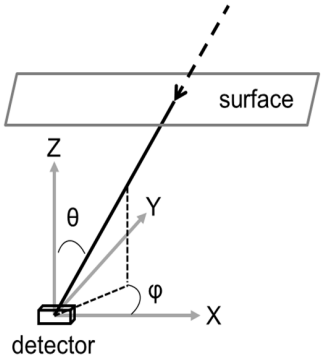

(b)

Figure 1: (a) An illustration showing muon rays from varying angles reaching the detector. A deposit with a high density contrast will cause a smaller muon flux (due to decay) than the surrounding geology. (b) The definitions of the angles at which a ray comes from the surface to the detector. The required angles for modelling are the dip (θ) and azimuth (φ).

structure. This model is created by known or assumed information from geology. If $\boldsymbol{\rho}_{ref}$ is a background reference model then the anomalous data are

$$\mathbf{d_a} = \mathbf{G}(\boldsymbol{\rho} - \boldsymbol{\rho}_{ref}) = \mathbf{G}\Delta\boldsymbol{\rho}. \tag{4}$$

As previously discussed, the muon data can be informative by themselves but jointly inverting traditional gravity along with the muon data should yield improved results. Therefore, we now turn to the gravity method to solve for density contrast.

GRAVITY DATA

Gravity surveys are commonly carried out and a large literature exists regarding acquisition, data reduction and inversion. Briefly, after data reduction, the vertical gravity for the i^{th} datum at location $\mathbf{r}_i$ is

$$d(\mathbf{r}_i) = \gamma \int_V \frac{z - z_i}{|\mathbf{r} - \mathbf{r}_i|^3} \Delta\rho(r) dv, \tag{5}$$

for anomalous density $\Delta\rho(\mathbf{r})$ throughout volume V (Blakely, 1996). The earth is discretized into the same prismatic volumes as the muon ray paths. The discretized problem can be expressed through equation 2, but where the sensitivity matrix for the i^{th} datum given the j^{th} model cell is given by

$$\mathbf{G}_{ij} = \gamma \int_{\Delta V_j} \frac{z - z_i}{|\mathbf{r} - \mathbf{r}_i|^3} dv, \tag{6}$$

and is expressed through vector notation by equation 3.

The 3D inversion of these data to estimate the anomalous density is routinely carried out (e.g. Li and Oldenburg (1998)).

JOINT INVERSION METHODOLOGY

With the same discretized model parameters, the combination of equations 1 and 5 creates the forward modelling for the joint inversion:

$$\begin{bmatrix} \mathbf{d}^m \\ \mathbf{d}^g \end{bmatrix} = \begin{bmatrix} \mathbf{G}^m \\ \mathbf{G}^g \end{bmatrix} \Delta\boldsymbol{\rho}, \tag{7}$$

but where $\mathbf{d} = (d_1^m, \ldots, d_{n_m}^m, d_1^g, \ldots, d_{n_g}^g)^T$ is a composite data vector containing n_m number of muon and n_g number gravity data. The sensitivity matrix is $n \times m$ for m prismatic volumes within the mesh and where $n = n_m + n_g$. The linear inverse problem is formulated as a minimization of a global objective function subject to the data constraints for both types of data (Menke, 1989; Parker, 1994). This is achieved through Tikhonov formalism (Tikhonov and Arsenin, 1977).

SYNTHETIC EXAMPLE

A synthetic example of a 3.17 g/cm^3 block at 150 m of depth representing a deposit in a 2.67 g/cm^3 half space is created to mimic the scenario. The resulting density contrast is g/cm^3. Five muon detectors are placed in a "tunnel" underneath the block (Figure 2).

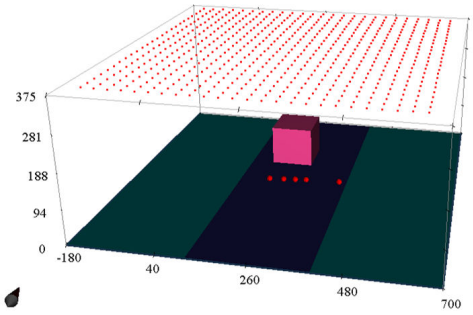

Figure 2: The true model of a block in a half space. The background rock is 2.67 g/cm^3 and the anomalous density of the block is 3.17 g/cm^3. Five muon detectors are placed below the block and are shown by the red spheres. The detectors are labelled 1-5 from west to east. Simulated gravity observation locations are shown as red dots on the surface. The anomalous density contrast of 0.5 g/cm^3 is used to model the gravity data.

To simulate field observations, muon ray paths are observed at approximately every 5° in azimuth and 2° dip from 1° to 35° from vertical. These numbers translate to 81 and 17 azimuth and dip angles, respectively for a single detector. Figure 3 shows the raypaths of the muon data discretized to the mesh.

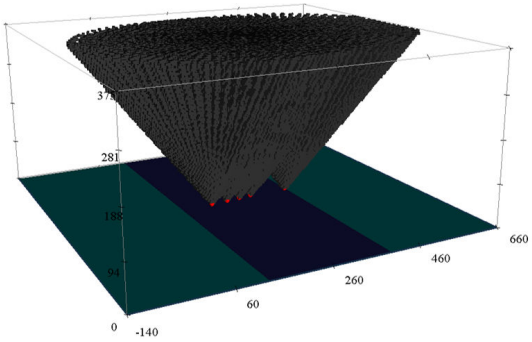

Figure 3: Muon ray paths that intersect the detectors (red spheres) are discretized into prismatic cells. The prisms with non-zero sensitivities for the 6885 muon ray paths are shown. The ray paths deviate as much as 35° from vertical.

Five percent Gaussian noise is added to the 6885 muon data. The simulated data are shown in Figure 4; it is typical to examine muon data through each detector as a function of angle. The dip, θ, is degrees from vertical. The azimuth, φ, is at 0° pointing the east. It is important to note that the data are integrated density along a ray-path length and therefore the overall data mimics the ray-path length. This is why smaller values are present at near-vertical dip angles. This type of visual inspection can be valuable when assessing the raw data when topography is present.

Next, we assume a background density of 2.67 g/cm^3. Following equation 4, the data are now assumed to arise solely from the anomalous density contrast, $\Delta\rho$. The data are shown in Figure 5. The noise in the simulated anomalous data are similar in magnitude to the actual signal; this emulates circumstances that can occur in field data. High values in the bottom panel of Figure 5 from $-10° < \varphi < 50°$ are the positive anomaly from the block. It should be noted that the effect from the block changes shape throughout the panels and is dependent upon the location of the deposit with respect to the sensor. The anomaly is located in the near-vertical angles throughout all azimuths in the third panel. The anomalous data are inverted. Figures 6(a) and 6(b) show a slice of the true model and recovered model from the muon anomalous data, respectively. The recovered density contrast is well located in the horizontal directions but smeared vertically. The maximum recovered density contrast is approximately 0.14 g/cm^3 which is somewhat less than the true anomalous density.

Gravity data are simulated at the surface and their locations are indicated by the red dots in Figure 2). There are 625 gravity data and five percent Gaussian noise has been added (Figure 7). In this case, the data values are very small, on the order of

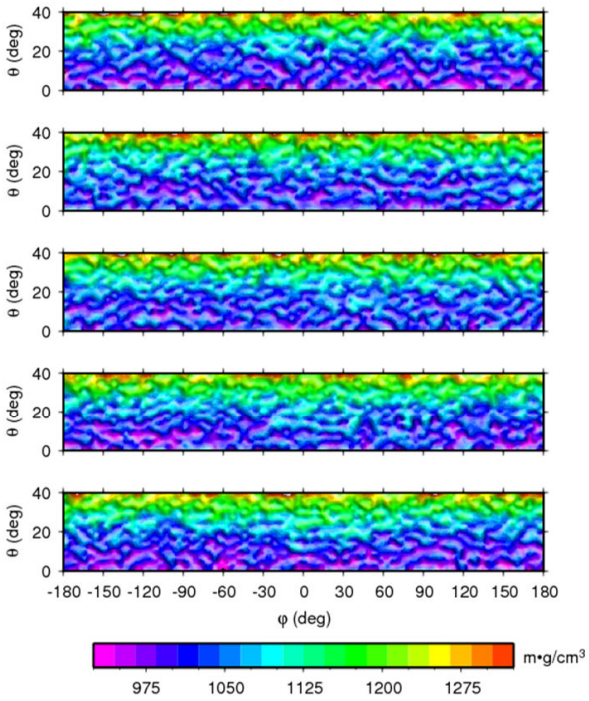

Figure 4: Muon data from the west-most receiver (top) to the east-most receiver (bottom). The ordinate is in degrees from vertical and the abscissa is in degrees around the azimuth with 0° pointing in the east direction. The trend of the data is due to the geometry involved.

tens of microgals. Anomalies with this magnitude are at the limit of detectability unless a carefully planned micro-gravity survey was carried out. Nevertheless, these data are inverted and the recovered model is shown in Figure 6(c). The shape of the anomaly is spherical and centred close to the true anomalous density. The anomalous mass is spread out and has a low amplitude. This is a common result in finding smooth models.

Joint inversion of both data sets is performed. The number of muon data influences the model by constraining the result laterally and recovering larger densities (Figure 6(d)). Though the gravity data are small in magnitude, they still provide valuable information. The gravity data forces the model deeper to reproduce the simulated data. Overall, positive qualities of both methods have been brought out. The combination of the two types of data has increased the accuracy and resolution of the recovered models as compared to either method alone.

CONCLUSION

Muon tomography is a new survey for mineral exploration. Here we have outlined the basic method of the survey and developed an inversion algorithm. Synthetic tests have been completed and the field data will be analysed this summer.

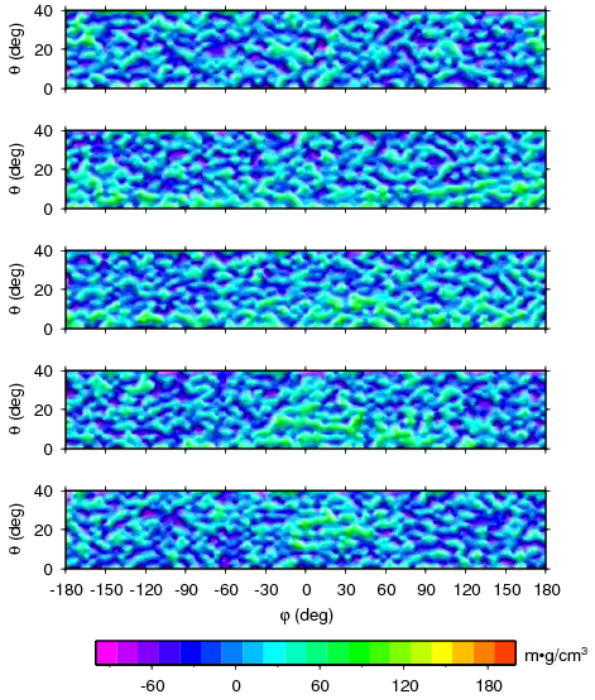

Figure 5: Anomalous muon data from the west-most receiver (top) to the east-most receiver (bottom). The ordinate is in degrees from vertical and the abscissa is in degrees around the azimuth with 0° pointing in the east direction. Data are in units of m·g/cm^3.

As with any geophysical technique, additional information can greatly reduce the inherent non-uniqueness and we illustrate this by jointly inverting the muon data with conventional gravity data. The two data sets provide complementary information. A synthetic example illustrates the different types of data and sets the stage for joint inversions of field data.

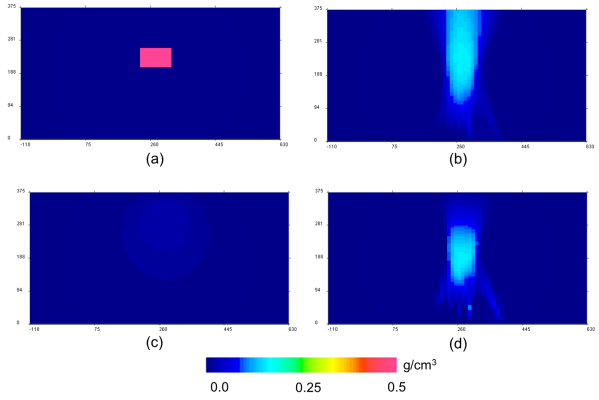

Figure 6: (a) A slice of the true model for comparison. Recovered models from the inversion of (b) muon tomography, (c) gravity, and (d) both gravity and muon tomography. The colour bars are consistent throughout the figure ranging from 0 to 0.5 g/cm^3.

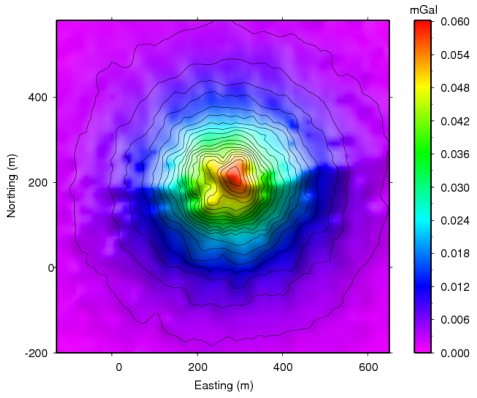

Figure 7: Simulated gravity data from a block with a density contrast of 0.5 g/cm,^{3} at a depth of 250 m.

REFERENCES

Alvarez, L. W., J. A. Anderson, F. E. Bedwci, J. Burhard, A. Fakhry, A. Girgis, F. Hassan, D. Iverson, G. Lynch, Z. Miligy, A. H. Moussa, M. Sharkawi, and L. Yazolino, 1970, Search for hidden chambers in the pyramids using cosmic rays: Science, **167**, 832–839.

Blakely, R., 1996, Potential theory in gravity and magnetic applications: Cambridge University Press.

Li, Y., and D. W. Oldenburg, 1998, 3-d inversion of gravity data: Geophysics, **63**, no. 1, 109–119.

Menke, W., 1989, Geophysical data analysis: discrete inverse theory: Academic Press.

Parker, R. L., 1994, Geophysical inverse theory: Princeton University Press.

Priedhorsky, W. C., K. N. Borozdin, G. E. Hogan, C. Morris, A. Saunders, L. J. Schultz, and M. E. Teasdale, 2003, Detection of high-z objects using multiple scattering of cosmic ray muons: Review of science instruments, **74**, no. 10, 4294–4298.

Schultz, L. J., K. N. Borozdin, J. J. Gomez, G. E. Hogan, J. A. McGill, C. L. Morris, W. C. Priedhorsky, A. Suanders, and M. E. Teasdale, 2004, Image reconstruction and material z discrimination via cosmic ray muon radiography: Nuclear instruments and methods in physics research. Section A, accelerators, spectrometers, detectors and associated equipment, **519**, no. 3, 687–694.

Tanaka, H. K. M., H. Taira, T. Uchida, M. Tanaka, M. Takeo, T. Ohminato, Y. Aoki, R. Nishitama, D. Shoji, and H. Tsuiji, 2010, Three-dimensional computational axial tomography scan of a volcano with cosmic ray muon radiography: Journal of Geophysical Research, **115**, B12332.

Tikhonov, A. N., and V. Y. Arsenin, 1977, Solution of Ill-posed Problems: Winston Press.

Wang, G., L. J. Schultz, and J. Qi, 2009, Bayesian image reconstruction for improving detection performance of muon tomography: IEEE transactions on image processing, **18**, no. 5, 1080–1089.